Draft version February 19, 2016
Preprint typeset using LaTeX style emulateapj v. 5/2/11

arXiv:1602.05903v1 [astro-ph.GA] 18 Feb 2016

THE MAGNETIZED GALACTIC WIND AND SYNCHROTRON HALO OF THE STARBURST DWARF GALAXY IC 10

Krzysztof T. Chyży[1], Robert T. Drzazga[1], Rainer Beck[2], Marek Urbanik[1], Volker Heesen[3], and Dominik J. Bomans[4]

Draft version February 19, 2016

ABSTRACT

We aim to explore whether strong magnetic fields can be effectively generated in low-mass dwarf galaxies and, if so, whether such fields can be affected by galactic outflows and spread out into the intergalactic medium (IGM). We performed a radio continuum polarimetry study of IC 10, the nearest starbursting dwarf galaxy, using a combination of multifrequency interferometric (VLA) and single-dish (Effelsberg) observations. VLA observations at 1.43 GHz reveal an extensive and almost spherical radio halo of IC 10 in total intensity, extending twice more than the infrared-emitting galactic disk. The halo is magnetized with a magnetic field strength of 7 μG in the outermost parts. Locally, the magnetic field reaches about 29 μG in H II complexes, becomes more ordered, and weakens to 22 μG in the synchrotron superbubble and to 7–10 μG within H I holes. At the higher frequency of 4.86 GHz, we found a large-scale magnetic field structure of X-shaped morphology, similar to that observed in several edge-on spiral galaxies. The X-shaped magnetic structure can be caused by the galactic wind, advecting magnetic fields injected into the interstellar medium by stellar winds and supernova explosions. The radio continuum scale heights at 1.43 GHz indicate the bulk speed of cosmic-ray electrons outflowing from H II complexes of about 60 km s^{-1}, exceeding the escape velocity of 40 km s^{-1}. Hence, the magnetized galactic wind in IC 10 inflates the extensive radio halo visible at 1.43 GHz and can seed the IGM with both random and ordered magnetic fields. These are signatures of intense material feedback onto the IGM, expected to be prevalent in the protogalaxies of the early Universe.

Subject headings: Galaxies: evolution – galaxies: magnetic fields – galaxies: dwarf – galaxies: irregular – galaxies: Local Group – radio continuum: galaxies – galaxies: individual: IC 10

1. INTRODUCTION

The generation, evolution, and role of magnetic fields in low-mass galaxies are still poorly understood. Massive late-type spiral galaxies are supposed to have suitable conditions to generate large-scale magnetic fields via the large-scale α–Ω dynamo (Beck et al. 1996). The interstellar medium (ISM) in these galaxies has sufficiently strong shearing motions, caused by a combination of differential rotation and the Coriolis force acting on turbulent gas motions. Low-mass, dwarf irregular galaxies have much more chaotic gas motions and slow rotation speeds with little rotational shear, which might be unsuitable for the generation of large-scale magnetic fields. The majority of massive spiral galaxies has spiral magnetic fields related to spiral density waves (Beck & Wielebinski 2013). In dwarf galaxies, without any coherent density wave structures, the magnetic field topology could potentially be very different and regulated by other processes.

In dwarfs with high star formation rates (SFRs), magnetic fields could be strongly modified by stellar winds, which constitute the dominant feedback in galaxy formation and evolution (Veilleux et al. 2005). Because low-mass objects have shallow gravitational potentials, they are easily subjected to large-scale (galactic) winds (Recchi & Hensler 2013). They are therefore suspected to potentially spread out magnetic fields and cosmic rays (CRs) far away from star-forming disks that may even pervade the intergalactic medium (IGM). Thus, they are among the best candidates for the cosmic magnetizers in the early Universe, where primordial galaxies may resemble some nearby starbursting low-mass galaxies (Kronberg et al. 1999; Dubois & Teyssier 2010). Still, we lack observational evidence that stellar feedback in starbursting dwarfs can indeed produce powerful galactic winds that are able to shape the global magnetic field structure.

One of the most nearby dwarf irregular galaxies, the Local Group member IC 10, is a very favorable target to test our current knowledge of the generation and evolution of magnetic fields in low-mass objects. The galaxy has a small linear size of about 1.6 kpc in diameter[5] and a low mass, for instance, the mass of neutral hydrogen of $M_{\rm HI} = 9.8 \times 10^7\ M_\odot$ is more than four times lower than that of the Small Magellanic Cloud (SMC; Grebel et al. 2003). IC 10 is remarkable for its high SFR and large number of H II regions (Hodge & Lee 1990). Normalized to its H_2 surface density, IC 10 has a much higher rate of star formation than most observed spiral or dwarf galaxies (Mateo 1998; Leroy et al. 2006). IC 10 has also a large population of Wolf-Rayet (W-R) stars and the highest surface density of W-R stars among all Local Group galaxies (Massey & Armandroff 1995). A high number of carbon-type W-R stars indicates that the galaxy experienced a brief, but intense, galaxy-wide burst of star formation within the last 10 Myr. The observed stellar population holds clues that the galaxy experienced another starburst in the past, ≈150–500 Myr ago (Vacca et al. 2007).

This galaxy shows a complex H I morphology and peculiar velocity field (Ashley at al. 2014). While the optical disk is aligned at a position angle of $PA = 125°$ and at an inclination angle of $i = 31°$ (according to the HyperLeda database), the H I disk has a different orientation: $PA \approx 75°$ and $i \approx 50°$

[1] Astronomical Observatory, Jagiellonian University, ul. Orla 171, 30-244 Kraków, Poland
[2] Max-Planck-Institut für Radioastronomie, Auf dem Hügel 69, 53121 Bonn, Germany
[3] School of Physics & Astronomy, University of Southampton, Southampton SO17 1BJ, UK
[4] Ruhr-Universität Bochum, Universitätsstrasse 150, 44780 Bochum, Germany

[5] We use the optical extent of IC 10 of 6.8′ from NED and the distance of 830 kpc from Sanna et al. (2008)

(Wilcots & Miller 1998). It shows that the ISM in IC 10 is highly disturbed and the galactic disk is only poorly defined. It is possible that IC 10 has merged with another dwarf galaxy and is accreting intergalactic gas filaments, which are visible in H I data cubes at various radial velocities. Both processes could have fed IC 10's disk and thereby triggered its current starburst.

IC 10 has also been investigated in the radio domain. In a polarization study by Chyży et al. (2003), using high-frequency (10.45 GHz), low-resolution (73″) single-dish observations, a single polarized region in the southern part of the galaxy was found, close to the position where Yang & Skillman (1993) found a large nonthermal superbubble. The rest of the disk of IC 10 was devoid of polarized signal. The studies of IC 10 were recently followed up by the high-resolution C-band JVLA observations of Heesen et al. (2011), which confirmed strong polarized emission in the region of the nonthermal superbubble. It was suggested that the ordered magnetic field can be enhanced by the gas compression of the expanding bubble. The superbubble can be powered by about 10 supernova explosions (Yang & Skillman 1993) or one hypernova event (Lozinskaya & Moiseev 2007). It is only a few Myr old and has yet to sweep up a shell of atomic hydrogen (Heesen et al. 2015). No other coherent polarized structures were found in IC 10 so far.

In this paper, we investigate the structure, origin, and evolution of the magnetic field in IC 10 utilizing sensitive multiband polarimetric observations obtained with the VLA and the 100-m Effelsberg telescope. Radio interferometers cannot detect emission at large angular scales, resulting in the so-called "missing spacings flux," which can be corrected for with single-dish observations. For instance, Heesen et al. (2011) found that in their JVLA observations of IC 10 at 6 GHz the flux density was ≈30% lower compared with the single-dish data presented by Chyży et al. (2003). The study presented here is based on a combination of VLA and Effelsberg data at 4.86 and 8.46 GHz, which allows us to study the largest angular scales found in weak, diffuse radio emission. Together with the VLA observations at 1.43 GHz, we are able to trace the synchrotron emission and magnetic fields not only in the galaxy's disk but also in its halo.

In Sect. 2 we present our radio observations of IC 10 and data reduction procedures. We present our results and their analysis in Sect. 3, followed by a discussion of the magnetic field structure and galactic wind (Sect. 4). In Sect. 5 we summarize our conclusions.

2. OBSERVATIONS AND DATA REDUCTION

2.1. *Effelsberg*

IC 10 was observed with the Effelsberg 100-m telescope[6] at 4.85 and 8.35 GHz. At 4.85 GHz we used the dual-horn system (at an angular horn separation of 8′) and a correlation polarimeter in the backend. Corrections to the telescope pointing model were made about every 1.5 hr by scanning a nearby strong unresolved radio source. The individual coverages were obtained in both azimuth and elevation directions. In order to establish a flux density scale, we observed the calibration source 3C 286 and assumed its total flux as 7.47 Jy, according to the flux scale established from VLA observations by Perley & Butler 2013).

[6] The 100-m telescope at Effelsberg is operated by the Max-Planck-Institut für Radioastronomie (MPIfR) on behalf of the Max-Planck-Gesellschaft.

The data were reduced in the NOD2 package (Haslam 1974), which allowed us to combine the coverages using software beam-switching (Emerson et al. 1979) and spatial-frequency weighting methods (Emerson & Gräve 1988). The maps were then digitally filtered to remove the spatial frequencies corresponding to noisy structures smaller than the telescope beam of 2.′5. The procedure of data reduction included masking of spurious emission of individual coverages and combining them into the final maps in Stokes parameters I,Q and U. Details of observations and the obtained rms noise levels are given in Table 1.

At 8.35 GHz the single-horn receiver in the secondary focus was used. High sensitivity of the observations was obtained by using a frequency bandwidth of 1.1 GHz. The galaxy was mapped employing scans along R.A. and Dec orientations. The calibrator 3C 286 was once again applied for the flux scale calibration, assuming 5.27 Jy total flux according to the VLA flux scale. We then combined individual coverages through a procedure similar as for 4.85 GHz, obtaining the final maps in Stokes I, Q and U with a resolution of 1.′4.

The final maps from both frequencies were converted to FITS format and taken into the Astronomical Image Processing System (AIPS)[7]. Maps of the total-power radio continuum intensity (TP), linearly polarized intensity (PI), degree of polarization, and E-vector orientation angles were thus obtained, and rms noise levels were determined (Table 1). The PI was corrected for the positive bias resulting from the Ricean distribution of noise. If not stated otherwise in the text, we present the magnetic field orientation, projected on the sky plane, as apparent B-vectors, which are defined as the E-vectors rotated by 90°, not corrected for Faraday rotation.

2.2. *VLA*

IC 10 was observed with the VLA[8] in L, C, and X band (Table 2). Observations were performed in the continuum mode (by now obsolete, after the upgrade to the WIDAR correlator) using a standard correlator setup with two IFs of 50 MHz bandwidth each, centered at 1385.100 and 1464.900 MHz, with all four correlations (*RR*, *LL*, *RL*, *LR*) recorded. We used J0059+581 as a phase calibrator to determine antenna gain solutions for amplitudes and phases, as well as the instrumental polarization leakages. As the primary calibrators, we used J0134+329 (3C 48) and J0518+165 (3C 138) to prescribe the flux scale and the absolute position angle of the polarization E-vectors.

We followed standard data reduction procedures using AIPS. The observations in all bands and configurations were first edited and calibrated separately and then self-calibrated in phase. Next, the data from all the observational sessions for a particular frequency band were combined and self-calibrated again. In the final stage, imaging with the AIPS task IMAGR was performed for all the Stokes parameters using Briggs's robust weighting of 1 and −5, where "robust=5" (−5) is equivalent to natural (uniform) weighting. The obtained Stokes Q and U maps were combined to form maps of polarized intensity, again corrected for the positive bias resulting from the Ricean noise distribution, and polarization angle. The obtained rms noise levels for total and polarized intensities are given in Table 2.

[7] AIPS, the Astronomical Image Processing Software, is free software available from the NRAO.

[8] The National Radio Astronomy Observatory is a facility of the National Science Foundation operated under cooperative agreement by Associated Universities, Inc. Karl G. Jansky Very Large Array (VLA)

TABLE 1
PARAMETERS OF THE EFFELSBERG OBSERVATIONS

Obs. Freq. GHz	Obs. Date	No. of Col/Rows in Coverages	No. of Coverages	S_{TP} (mJy)	S_{PI} (mJy)	rms (TP) (mJy beam^{-1})	rms (PI) (mJy beam^{-1})
4.85	2001	51 × 41	10	222 ± 9	6.3 ± 0.4	0.80	0.14
8.35	2003	33 × 33	22	183 ± 8	2.5 ± 0.5	0.50	0.072

TABLE 2
PARAMETERS OF THE VLA OBSERVATIONS

Band	Obs. Date	Configuration	Integr. Time (hr)	rms (TP) (mJy beam^{-1})	rms (PI) (mJy beam^{-1})
L	2004 Mar. 27 / 2004 Aug 15	C/D	5.0/4.3	28[a]	15[a]
C	2001 Dec. 4,28,31	D	24.2	17[b]	6.5[b]
X	2003 Feb. 9,10,14 / 2003 Apr. 11,12,27 / 2004 Aug. 18	D	37.1	10[b]	3.5[b]

[a] - Final rms noise level for the concatenated data from C and D configurations. [b] - rms noise levels for the merged VLA and Effelsberg data (see text).

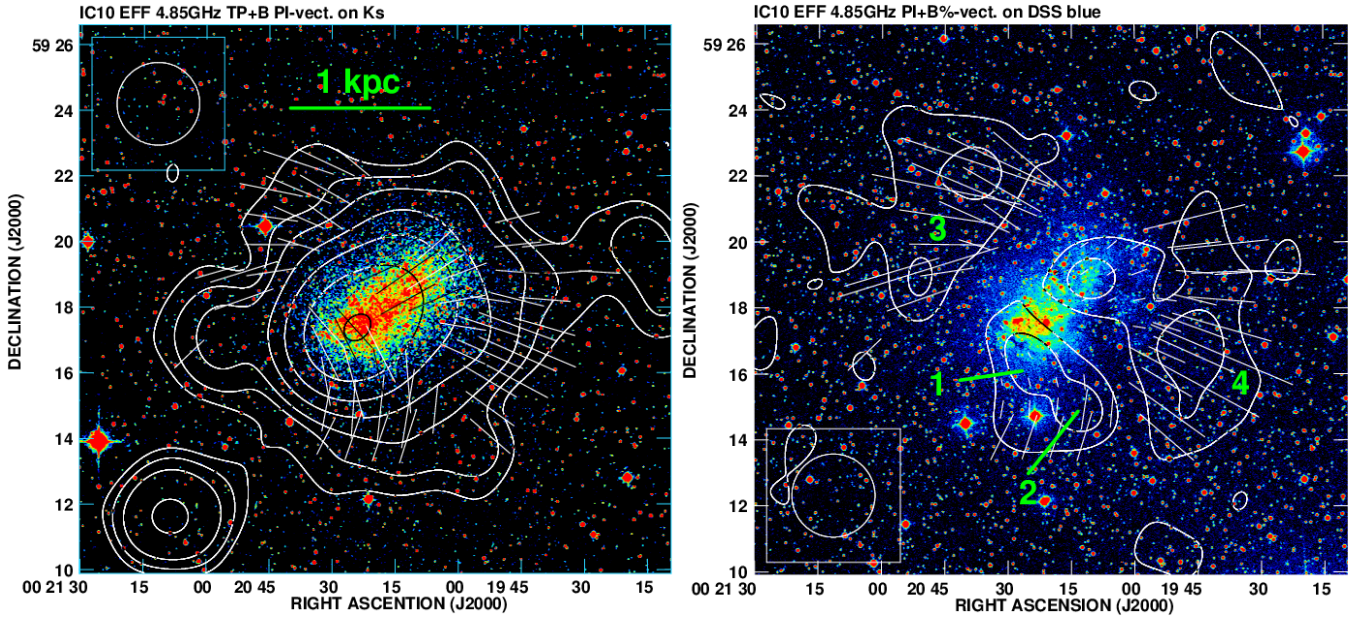

FIG. 1.— Left: total-power contours and B-vectors of polarized intensity of IC 10 at 4.85 GHz superimposed on the 2MASS Ks band (2.2 μm) image. The contours levels are (−3, 3, 5, 8, 16, 32, 64, 128) × 800 μJy beam^{-1}. A vector of 10″ length corresponds to a polarized intensity of 59 μJy beam^{-1}. Right: Contours of polarized intensity and B-vectors of polarization degree of IC 10 at 8.35 GHz superimposed on the DSS blue image. The contour levels are (3, 5) × 140 μJy beam^{-1}. A vector of 10″ length corresponds to a polarization degree of 1%. The resolution of the maps is 151″ × 151″ HPBW.

As IC 10 has a relatively large angular optical size (≈7′), interferometric observations may lead to missing large-scale structure and underestimation of the galaxy's flux (cf. Sect. 1). In order to eliminate this effect, the data from VLA and Effelsberg in C and X bands were merged. The merging was performed within the Miriad package (Sault et al. 1995, task IMMERGE). The radio maps obtained in this way for I, Q and U Stokes parameters, PI, and polarization angle were used in the further analysis (Sect. 3).

3. RESULTS

3.1. *Low-resolution data*

In Figure 1 we present the total-power map of IC 10 from the Effelsberg observations at 4.85 GHz. The bright radio emission is morphologically oriented along the optical main body of the galaxy, the maximum corresponding to the giant H II region in the south, well visible in the image in blue optical color. The low-level emission (at 3–5 times the noise level) extends far away from the galaxy's main stellar body in each direction. The three farthest elongations of the radio emission are background sources at R.A.(J2000)=$00^h19^m15\overset{s}{.}0$, decl.(J2000)=59°19′00″; R.A.=$00^h21^m0\overset{s}{.}8$, decl.=59°16′59″, and R.A.=$00^h20^m8\overset{s}{.}7$, decl.=59°13′27″), well visible in the high-resolution NVSS map and our VLA map at 1.43 GHz (see below). Another background source, located farther away and detached from the disk, is located at R.A.=$00^h21^m10\overset{s}{.}0$, decl.=59°11′30″.

The PI at 4.86 GHz is distributed into several major regions (Fig. 1, right panel). The first of them is located in the southern part of the brightest H II region. Emission at this place was also observed by Chyży et al. (2003) at 10.45 GHz. The orientations of B-vectors in both data sets are similar in this

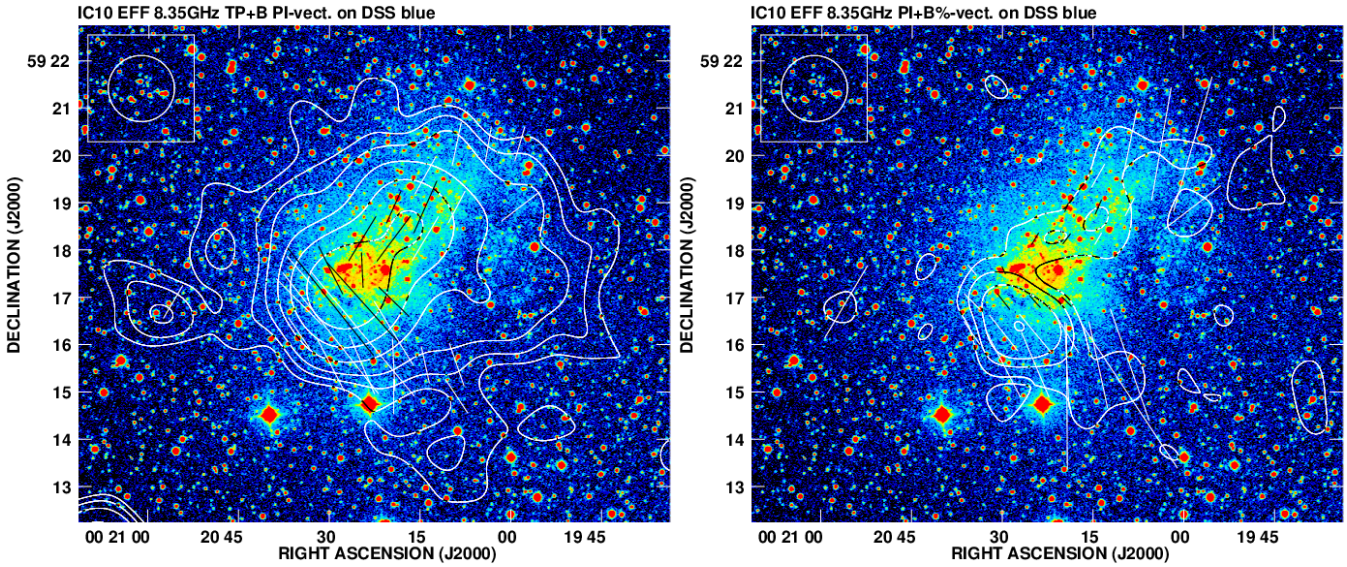

FIG. 2.— Left: total-power contours and B-vectors of polarized intensity of IC 10 at 8.35 GHz superimposed on a DSS blue image. The contour levels are (−3, 3, 5, 8, 16, 32, 64) × 500 μJy beam^{-1}. A vector of 10″ length corresponds to a polarized intensity of 50 μJy beam^{-1}. Right: contours of polarized intensity and B-vectors of polarization degree of IC 10 at 8.35 GHz superimposed on a DSS blue image. The contour levels are (3, 5, 8, 16) × 72 μJy beam^{-1}. A vector of 10″ length corresponds to a polarization degree of 0.7%. The resolution of the maps is 84″ × 84″ HPBW.

region and perpendicular to the galaxy's optical major axis (with $PA = 125°$, but notice that the disk definition is uncertain for IC 10; see Sect. 1). However, in the 4.85 GHz data an additional component (No. 2 in Fig. 1) with a "radial" orientation of B-vectors can also be seen. Another region of PI covers the northwest portion of the optical disk and shows B-vectors roughly aligned with it. A hint of such a magnetic field was found by Heesen et al. (2011) in their C-band JVLA observations of IC 10. The other two PI regions (3 and 4) are located at the outskirts of the radio total emission up to about 1 kpc distance from the optical edge of the disk. The B-vectors in these regions have a coherent pattern, with mostly radial orientations relative to the major axis of the optical disk. The characteristic valley in the PI visible in the east part of IC 10, between the disk and the polarized component (3), is likely due to the effect of beam depolarization caused by perpendicular orientations of the magnetic fields in the disk and galactic outskirts. It turns out that this galaxy, despite its small linear size, possesses a halo of weak, diffuse polarized emission, not detected in previous studies (Chyży et al. 2003; Heesen et al. 2011).

The total-power flux at 4.85 GHz integrated over the whole radio extent of the galaxy is 222 ± 9 mJy (Table 1), leaving out the four background sources. Heesen et al. (2011) found a flux density of 145 mJy (extrapolated to 4.85 GHz) from their interferometric data, which are not sensitive to radio emission on large angular scales, which is 34% deficient compared with our Effelsberg maps. The polarized flux is 6.3±0.4 mJy, which results in a polarization degree of 2.8% ± 0.2 %.

In Fig. 2 a higher-resolution (84″) radio map of IC 10 from the Effelsberg data at 8.35 GHz is shown. Similarly to 4.85 GHz, the maximum of emission again coincides with the brightest H II complex in the galaxy and the strong emission is found along the galaxy disk. Furthermore, a characteristic diffuse emission to the west of the optical disk is visible, covering a long chain (up to 3′ in length) of Hα-emitting filaments. The map confirms similar features found at 10.45 GHz by Chyży et al. (2003).

In the PI map (Fig. 2, right) there is a clear maximum of emission corresponding to region 1 in the 4.85 GHz map (Fig. 1). The peak has no bright Hα counterpart, but coincides with the nonthermal superbubble of 48″ size, found there at R.A.=$00^{\rm h}20^{\rm m}28\overset{\rm s}{.}0$, decl.=59°16′48″ by Yang & Skillman (1993). The orientation of the B-vectors in this region is similar to those observed at 4.85 GHz, which suggests no strong Faraday rotation effects there (see Sect. 3.4). There are some patches of polarized emission along the optical disk at 8.35 GHz; however, no extraplanar (diffuse) polarized signal is observed, in contrast to the 4.85 GHz detection in regions 3 and 4.

The integration of total radio emission gives a total-power flux at 8.35 GHz of 183 ± 8 mJy and a polarized flux of 2.5 ± 0.5 mJy. The average degree of polarization is 1.4%, slightly lower than at 4.85 GHz, which is probably due to less extended emission observed at 8.35 GHz (e.g. no detection of polarized emission in regions 3 and 4 that are seen at 4.85 GHz).

3.2. *High-resolution Data*

3.2.1. *Synchrotron Envelope at 1.43 GHz*

The sensitive low-frequency VLA observations of IC 10 at 1.43 GHz reveal a very extended total-power radio emission of the object (Fig. 3, left). The envelope extends to about 1.4 kpc (6′) in radius, much further than the stellar disk visible in Ks-band (Fig. 1) and all the radio continuum emission at various frequencies published to date. We do not find matching Hα-emiting gas, but this can suffer from strong foreground extinction (the galactic latitude of IC 10 is about $-3\overset{\circ}{.}3$). Because also the comparison of infrared emission observed by *Spitzer* at 24 μm does not reveal the galaxy envelope to the extent visible at 1.43 GHz (actually, the infrared-emitting disk is roughly two times smaller; Figure 4, left panel), the envelope must be of nonthermal origin (see also Sect. 3.3).

We note that the galaxy in the 1.43 GHz map is surrounded by a weak "negative bowl," indicating that missing zero spacings may prevent the detection of some very extended emission even at 1.43 GHz. Therefore, we suspect that the radio envelope of IC 10 could be actually even larger. Much lower

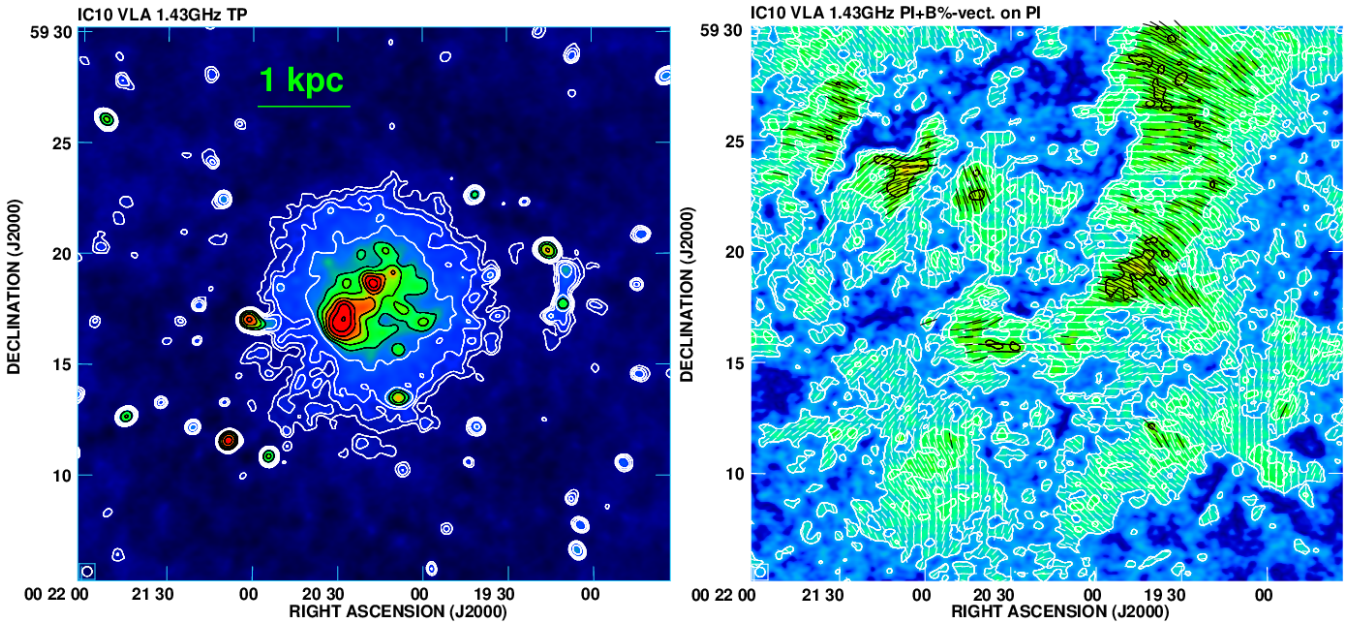

FIG. 3.— Left: total-power contours of IC 10 at 1.43 GHz superimposed on the total-power image. The contour levels are (3, 5, 8, 16, 32, 64, 128, 256, 512, 1024) × 28 μJy beam^{-1}. Right: contours and B-vectors of polarized intensity of IC 10 at 1.43 GHz superimposed on the polarized intensity map. The contour levels are (3, 5, 8) × 15μJy beam^{-1}. A vector of 10″ length corresponds to a polarized intensity of 25 μJy beam^{-1}. The resolution of the 1.43 GHz radio maps is 26″ × 26″ HPBW.

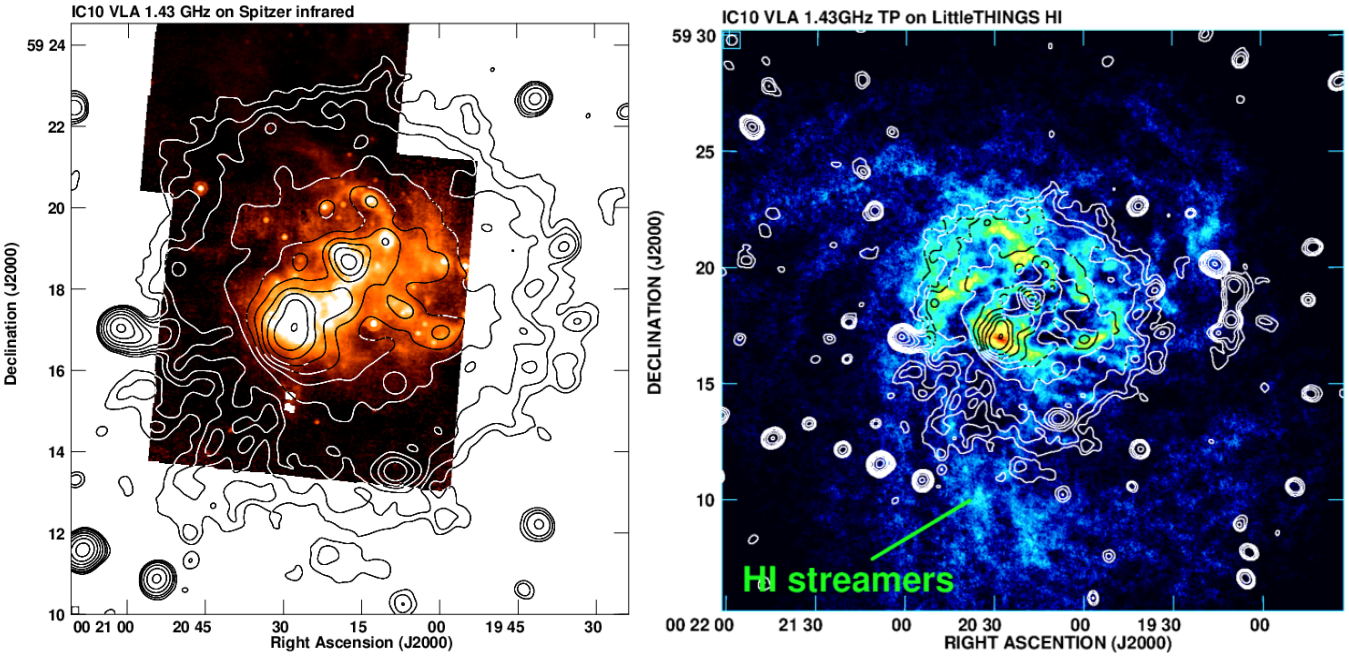

FIG. 4.— Left: total-power contours of IC 10 at 1.43 GHz (see Fig. 3, left panel) superimposed on the *Spitzer* map at 24 μm (Bendo et al. 2012). The *Spitzer* map resolution is 5.″3 × 5.″3 HPBW. Right: total-power contours of IC 10 at 1.43 GHz (see Fig. 3, left panel) superimposed on the H I map (Hunter et al. 2012). The H I map resolution is 8.″44 × 7.″45 HPBW.

frequency observations are needed, e.g., with LOFAR to determine the full extent of the synchrotron halo in IC 10. Low frequencies are preferred as they can reveal synchrotron emission generated by an old population of CR electrons spiraling along weak magnetic fields far away from star-forming regions.

The synchrotron envelope of IC 10 is quite symmetric and smooth. While it extends farther than the distributions of main bulk of young and old stars, traced by *Spitzer* 24 μm and the Ks-band data, its size in the east-west direction is similar to that of the neutral hydrogen (Fig. 3). Farther away from the disk, where a network of H I streamers and extensions can be seen, there are no traces of radio signal. The H I data reveal many complex structures that result from some counterrotating components within the disk (Wilcots & Miller 1998) and remnants of past gravitational interaction (Ashley at al. 2014; Nidever et al. 2013). The synchrotron emission seems not to be associated with the H I features and has its own more symmetrical morphology.

The total-power flux of IC 10 measured at 1.43 GHz is 377±

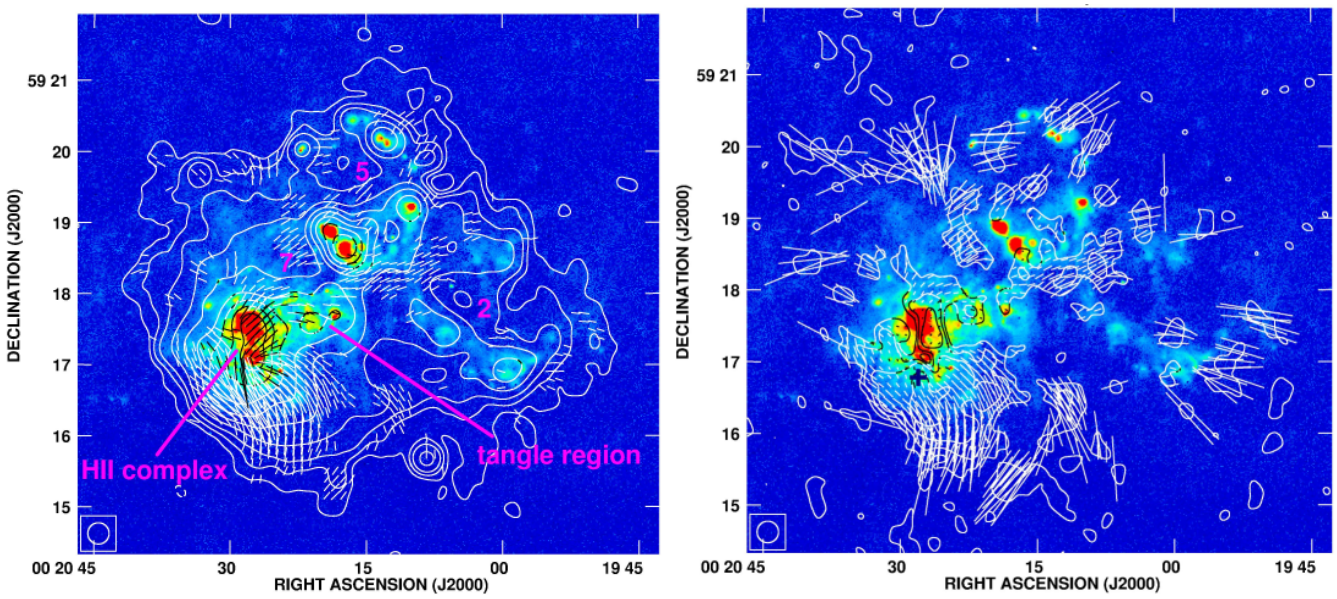

FIG. 5.— Left: total-power contours and B-vectors of polarized intensity of IC 10 (from the combined VLA and Effelsberg data) at 4.86 GHz superimposed on an Hα image (Gil de Paz et al. 2003). The contour levels are $(-3, 3, 5, 8, 16, 32, 64, 128, 256, 512) \times 17\,\mu$Jy beam^{-1}. A vector of 10″ length corresponds to a polarized intensity of about $33\,\mu$Jy beam^{-1}. The map resolution is 18.″0 × 18.″0 HPBW. H I holes 2, 5, and 7 are denoted (see Wilcots & Miller 1998). Right: contours of polarized intensity and B-vectors of polarization degree of IC 10 (from combined VLA and Effelsberg data) at 4.86 GHz superimposed on an Hα image (Gil de Paz et al. 2003). The contour levels are $(3, 5, 8, 16) \times 6.5\,\mu$Jy beam^{-1}. A vector of 10″ length corresponds to a polarization degree of 6.25%. The map resolution is 18.″0 × 18.″0 HPBW. The synchrotron superbubble is marked by a cross. The linear size of the superbubble is 48″.

11 mJy.

3.2.2. *Milky Way Contribution in Polarized Signal at 1.43 GHz*

The distribution of the PI of IC 10 at 1.43 GHz is another surprise of this galaxy (Fig. 3, right). There is a lot of polarized signal visible in the map, but it is not directly related to IC 10. In fact, the entire primary beam of the telescope is filled with patches of diffuse polarized signal at a level of at least $45\,\mu$Jy beam^{-1}. This, combined with the galactic latitude of IC 10, which is about $-3.^{\circ}3$, leads one to suspect that the observed PI possibly comes from the Milky Way. It has been difficult to assess on the basis of the available data whether there is actually any polarized emission at 1.43 GHz coming from IC 10. New wideband VLA observations, e.g. in L band (1–2 GHz), and application of the rotation measure (RM) synthesis technique, which for this frequency range would result in a Faraday depth resolution of about 40 rad m^{-2}, may allow us to separate the Milky Way foreground contribution from IC 10.

These findings are quite peculiar ones, constituting the strongest manifestation of Milky Way foreground emission in observations of any external galaxy yet. A hint of additional polarized signal not directly related to the investigated galaxy was found in NGC 7331, which is located significantly farther away from the Galactic plane ($-20.^{\circ}7$) than IC 10 (Heald et al. 2009). Detection of strong polarized emission from the Milky Way portends difficulties in obtaining and interpreting polarized signals from galaxies observed at extremely low radio frequencies, now starting to be covered by the LOFAR instrument (Mulcahy et al. 2014).

3.2.3. *High-frequency Data and X-shaped Halo Field*

The total-power high-resolution (18″) map obtained from the combined VLA and Effelsberg data at 4.86 GHz is presented in Fig. 5 (left), superimposed on an Hα image. Many radio intensity maxima correspond well to the bright H II regions. A more diffuse-like emission fills the entire optical disk and extends farther to the northeast and southwest. Only the southeastern edge of the disk does not show such extension; - here the radio emission quickly drops to the noise level. This is surprising as this region is very close to the giant H II complex where one would expect an efficient production of CR electrons. Something must prevent diffusion of CRs into this direction.

In Fig. 5 the PI map from the combined VLA and Effelsberg data at 4.86 GHz is presented. The most prominent polarized signal found in the object is located to the south and southwest of the giant H II complex. While the orientations of the B-vectors are perpendicular to the galactic major axis in this region, they subsequently change to radial orientations in the area farther to the south. The same pattern could be discerned in the Heesen et al. (2011) data, but here the polarization is also visible in other regions. Beyond the southern part of the galaxy, the distribution of the PI is patchy and apparently avoids any star-forming sites. H II regions actively form massive stars and produce enhanced turbulent motions that can effectively destroy ordered magnetic fields. We find a similar process at work in the spiral arms of massive galaxies (e.g. Chyży et al. 2007b).

The analysis of the degree of polarization confirms this finding. The highest degrees of polarization, reaching values of up to 50%, are found in regions of low star formation activity, i.e. in the outskirts of the galaxy. In the nonthermal superbubble, we find values of ≈25%. The lowest degree of polarization of about 0.5% is coincident with the giant H II complex. The polarized flux measured for the whole galaxy at 4.86 GHz is 4.9 ± 0.6 mJy, which results in a mean polarization degree of 2.6% ± 0.3 %.

In order to obtain a clearer global picture of the distribution of the PI in IC 10, we convolved the PI map with a Gaussian kernel to a lower angular resolution of 45″ (Fig. 6). Astonishingly, a pattern of global magnetic fields emerges in this dwarf irregular galaxy, extending far beyond the optical disk into the halo! In its farthest extensions, found northeast and

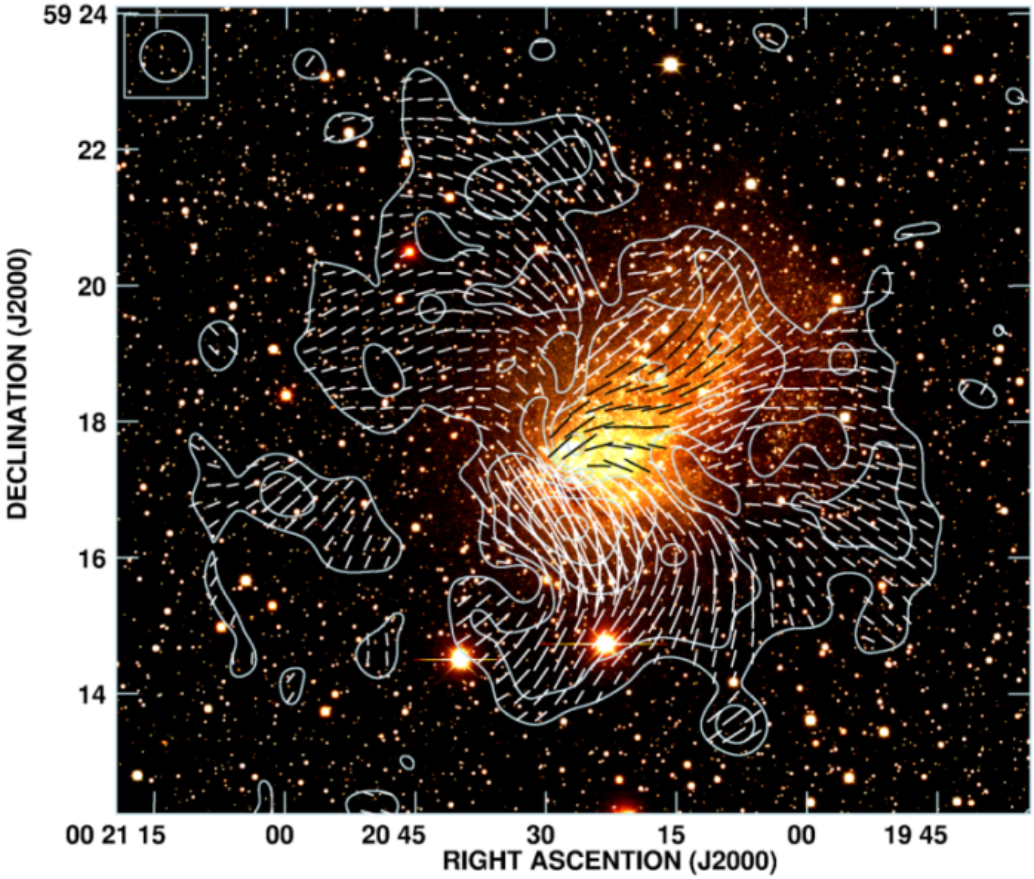

FIG. 6.— Contours and B-vectors of polarized intensity (from combined VLA and Effelsberg data) of IC 10 convolved to the resolution of 45″ at 4.86 GHz and superimposed on the true-color optical image (from P. Massey/Lowell Observatory and K. Olsen/NOAO/AURA/NSF). The contour levels are (3, 6, 12, 24, 40) × 11 μJy beam^{-1}. A vector of 10″ length corresponds to a polarized intensity of about 38 μJy beam^{-1}.

southwest of the main stellar body, the orientations of the B-vectors are radial, suggesting the presence of a halo magnetic field. The ordered magnetic field pointing away from the center of the galaxy displays a partly distorted "X-shaped" morphology. Note that this structure is also seen in Fig. 1. There is also a quite distinct magnetic field component aligned with the main optical body of the galaxy (PA = 125°). X-shaped halo magnetic fields have so far been found only in late-type spiral edge-on galaxies (e.g. Soida et al. 2011), but they have never been detected in any dwarf irregular galaxy. The magnetic structure of IC 10 partly resembles the X-pattern in the late-type spiral galaxy NGC 4631, which possesses a large radio halo with radial field lines advected in a strong galactic wind (Mora & Krause 2013). See Sect. 4.2 for further discussion.

In Figure 7, we present the total-power radio continuum map of IC 10 at 8.46 GHz, which has the highest linear resolution (44 pc) of all the maps included in this work. The corresponding map of the linear polarization (Fig. 7) is the most sensitive image (3.5 μJy beam^{-1}) obtained for this object to date. Both the total and PI distributions are very similar to those at 4.86 GHz (compare Fig. 5). As for the 4.86 GHz data, there is an apparent anticorrelation between the PI and the bright H II complexes in the disk, whereas the opposite is observed for the total intensity. We find the same situation in the so-called "tangle region" of Thurow & Wilcots (2005), which is composed of many distinct, compact H II regions immersed in diffuse Hα emission. Weak polarized emission is detectable at the edges of this region and reveals magnetic field vectors directed outward from this area (Fig. 7).

The bulk of the polarized emission is found in the region of the nonthermal superbubble and the area adjacent to the southwest. Here the field lines are probably unrelated to the superbubble as they cross the bubble from northeast to southwest and continue farther to the south. The B-vector orientations mostly agree with those at 4.86 GHz, indicating that Faraday rotation is small and we observe the intrinsic magnetic field orientation.

From the high-resolution data at 8.46 GHz we find integrated flux densities of 154 ± 4 mJy and 4.1 ± 0.3 mJy, for total-power and polarization, respectively. Hence, the mean degree of polarization is 2.7% ± 0.2 %. The spatially resolved degree of polarization has its minimum with 2–3% close to the giant H II complex, whereas the maximum values are found close to the southern edge of the halo with values of ≈30%. Such a high degree of polarization could be caused by either compression or stretching of magnetic field lines. Both processes may be active in this area, whereas they are suppressed in the nearby giant H II complex. Gravitational interaction or gas accretion can cause gaseous streamers and bulk flows of H I gas, leading to compression and stretching of the magnetic field lines (see Sect. 4.2).

3.3. *Distribution of Spectral Index and Nonthermal Emission*

In Fig. 8 we present the spectral index distribution between 1.43 GHz (imaged with robust 0) and 4.86 GHz (from the combined VLA and Effelsberg data). Both maps were first convolved to the common resolution of 19″ and clipped at intensities below 5 times the rms noise level. Flat spectral indices at −0.1 to −0.2 are cospatial with bright, compact H II regions, which suggests that they are dominated by thermal emission. Indeed, IC 10 is known to manifest a significant thermal fraction of radio emission (about 50% at 10.45 GHz; Chyży et al. 2003). Similar flat spectra were also observed

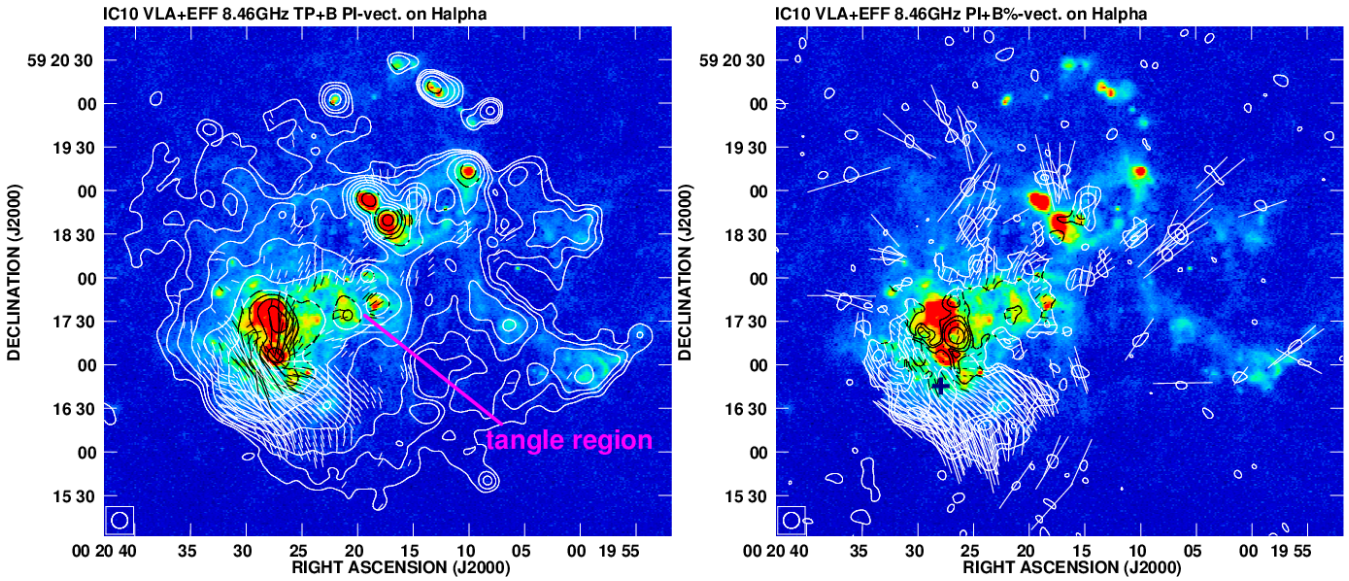
IC10 VLA+EFF 8.46GHz TP+B PI-vect. on Halpha
IC10 VLA+EFF 8.46GHz PI+B%-vect. on Halpha
DECLINATION (J2000)
RIGHT ASCENSION (J2000)
tangle region

FIG. 7.— Left: total-power contours and B-vectors of polarized intensity of IC 10 (from combined VLA and Effelsberg data) at 8.46 GHz superimposed on the Hα image (Gil de Paz et al. 2003). The contour levels are (−3, 3, 5, 8, 16, 32, 64, 128, 256, 512, 1024) × 10 μJy beam^{-1}. A vector of 10″ length corresponds to a polarized intensity of about 25 μJy beam^{-1} (not corrected for the primary beam attenuation). The map resolution is 11.″0 × 11.″0 HPBW. Right: contours of polarized intensity and B-vectors of polarization degree of IC 10 (from combined VLA and Effelsberg data) at 8.46 GHz superimposed on the Hα image (Gil de Paz et al. 2003). The contour levels are (3, 5, 8, 16) × 3.5 μJy beam^{-1}. A vector of 10″ length corresponds to the polarization degree of about 7.14%. The map resolution is 11″ HPBW.

by Heesen et al. (2011) in their high-resolution spectral index map obtained with the multifrequency synthesis method. However, their map is limited to just the galaxy's brightest part. In the spectral index map presented in this paper a more diffuse component of radio emission, located mainly in between star-forming regions, can also be discerned. Such regions show steeper spectral indices, ranging between −0.4 and −0.5, indicating a mix of nonthermal (synchrotron) and thermal (free–free) emission.

Toward the edges of the galaxy, the spectral index steepens to a value of about −1, which means that these regions are dominated by synchrotron emission. The same applies to the region of the nonthermal superbubble, where the spectral index has a value of about −0.8.

The spectral index map shows a northeast-southwest asymmetry across the optical disk with flatter spectral indices found on the southwestern side. Such a pronounced asymmetry is not visible in the 1.43 GHz total intensity map, indicating that the spectral asymmetry is due to strong thermal emission from regions of recent star formation on the southwestern side of the disk. Such emission comes particularly from the "tangle region" and from the long curved Hα extension (around R.A.=$00^{h}20^{m}00^{s}$, decl.=59°17′50″) filled with young shells and gas filaments.

A separation of the thermal and nonthermal components of the radio emission is essential for the determination of the magnetic field strength (Sect. 4.1) and for the analysis of the relation between the magnetic field and other ISM phases. In our approach we use the estimation of the mean Hα dust extinction from our previous paper of Chyży et al. (2003) to correct our Hα map for dust attenuation. The theory of free-free emission is then used (Caplan & Deharveng 1986) to derive from the corrected Hα map the predicted thermal radio flux map of IC 10 at 4.86 GHz. This map is then subtracted from the total radio map at 4.86 GHz to obtain the distribution of nonthermal emission (Fig. 9).

The nonthermal emission of IC 10 fills the entire optical

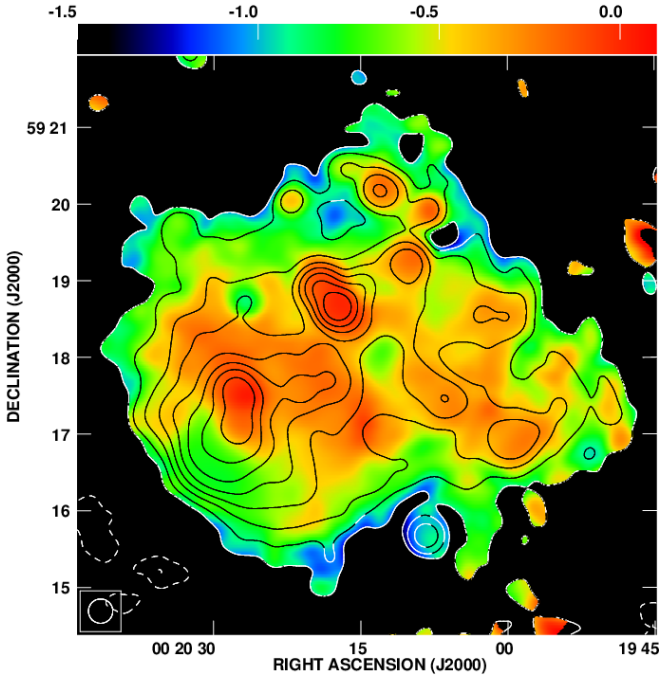

FIG. 8.— Radio spectral index distribution between 1.43 (Robust 0) and 4.86 GHz (merged VLA and Effelsberg data) in IC 10 (colors). Both the maps of total intensity were convolved to a common beam of 19″. The contours represent the total-power map at 4.86 GHz; the levels are (−5, −3, 5, 8, 16, 32, 64, 128, 256, 512) × 17 μJy beam^{-1}.

body of the galaxy, as found in star-forming spiral galaxies (e.g. Chyży et al. 2007a). It is particularly strong in the region of the nonthermal superbubble (as expected) and in the whole southern polarized region. However, it is also strong in the southern and northern H II complexes, hinting at a connection between star formation, production of CRs, and amplification of magnetic fields. Here the spectral index is flatter than in the polarized region. In the western area, there is a significant extension of nonthermal emission, which follows

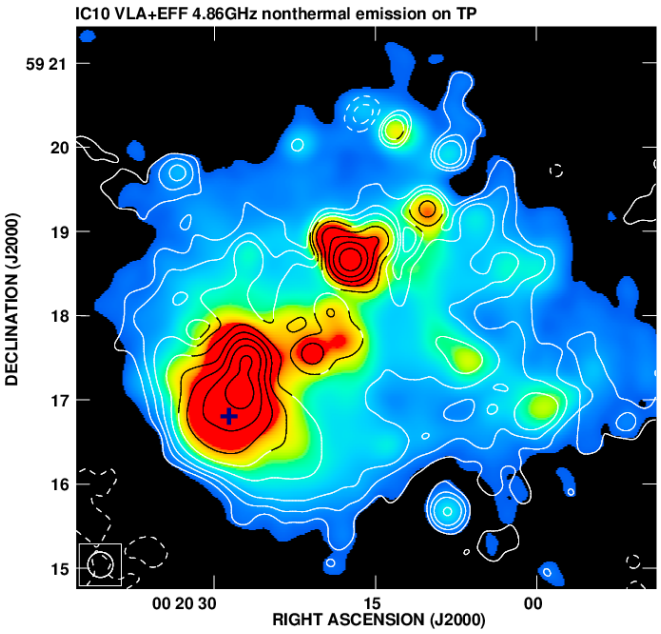

FIG. 9.— Distribution of nonthermal radio emission in contours superimposed on the total-power radio emission at 4.86 in IC 10. The contours levels are: (−5, −3, 3, 5, 8, 16, 32, 64, 128, 256) ×25 μJy beam^{-1}. The map resolution is 18″.

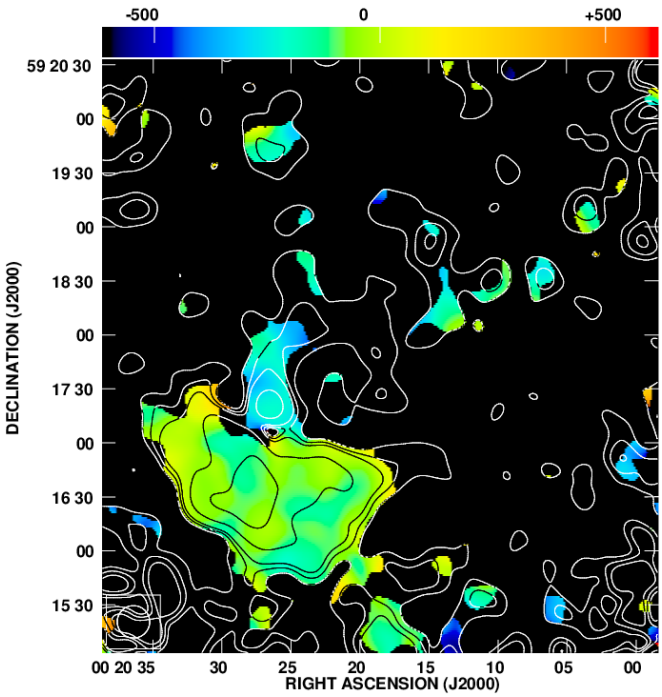

FIG. 10.— Distribution of Faraday RM in IC 10 (in rad m^{-2}, not corrected for the foreground RM) from the data at 4.86 and 8.46 GHz in IC 10 (colors). The contours represent the polarized intensity map at 8.46 GHz; the levels are: (4, 6, 8, 16, 32) × 8 μJy beam^{-1}. The map resolution is 18″.

the chain of H II regions. In contrast, the nonthermal emission in the opposite (northeastern) direction is weaker and extends only half as far out into the halo. In this area, there are also fewer H II regions, and hence also less sources able to produce CRs and synchrotron emission. This is clearly confirmed by the steeper spectral index on the northeastern side of the disk (Fig. 8). These findings are also supported by X-ray observations, - which show confined 10^6 K gas in the southern part and the main disk of IC 10 (Wang et al. 2005). The hot gas has probably already escaped from the western chain of (older) H II regions, as well as from the eastern galaxy part. In the southern part the population of W-R and other massive stars is still able to maintain the hot gas and balance the cooling of X-rays.

In contrast to the 4.86 GHz emission, we find that the 1.43 GHz emission, which is dominated by the nonthermal component, has a much higher degree of symmetry, forming an almost spherical halo. It would seem that an older population of CR electrons fill the radio envelope of IC 10 in a much more uniform way, requiring efficient CR transport. As will be shown in Sect. 4.3, the convection timescale for the CRs to be transported out to the edge of the halo at 1.5 kpc distance is 25 Myr (assuming a wind speed of about 60 km s^{-1}, see Sect. 4.3). The origin of the oldest CR electrons in the halo thus predates the current starburst and suggests that they are stemming from an earlier epoch of star formation (see Sect. 4.1).

3.4. *Distribution of RM*

In the present study, for the first time, we obtained a map of the RM distribution in IC 10 (Fig. 10). The map was calculated using the observations at 4.86 and 8.46 GHz convolved to a common angular resolution of 30″. Both polarization maps were clipped at intensities below 4 times the rms noise level. The resulting typical uncertainty of RM is about 68 rad m^{-2} for a signal-to-noise ratio of (S/N) of 4 and smaller for larger S/N. The most characteristic RM structure is a large region in the south of the galaxy corresponding to the nonthermal superbubble and the polarized extension to the southwest from it. In this area the RM is approximately −86±26 rad m^{-2}, with some variation over the whole region. In the southern giant H II complex it reaches values around −250 ± 33 rad m^{-2}. The RM distribution is more patchy in other regions. Large values of RM in the most southern location, at declinations below 16°, are due to an increased rms noise in the proximity of the primary beam edge at 8.46 GHz.

Nonvanishing absolute RM values, averaged in regions larger than the telescope beam, might suggest the existence of regular[9] magnetic fields in IC 10. This would shed a new light on the generation and evolution of the magnetic field in this object and challenge the current understanding of the magnetic field generation mechanism in dwarf galaxies (Chyży et al. 2003). However, IC 10 is located almost in the Milky Way's plane, which may contribute to the total RM signal, acting as a foreground Faraday screen. From the all-sky RM map of Oppermann et al. (2012) we found that for the Galactic coordinates of IC 10 the interpolated Galactic Faraday depth (foreground RM) is about −98±61 rad m^{-2}. Large uncertainty results from the low resolution of the map (about 0.5°) and variation of the Faraday depth close to the Galaxy plane. As this value is close to the one determined from our RM map in the direction of the superbubble, the Galactic foreground can almost fully explain the obtained RM signal, and we do not have any conclusive evidence for a regular magnetic field in IC 10.

After subtracting the foreground RM from the value determined for the giant H II complex, we obtain the residual value of about −150 ± 69 rad m^{-2}. This may arise from some local enhancement of the Milky Way foreground signal or might be intrinsic from within IC 10. Systematic negative values of RM indicate regular magnetic fields oriented mostly away from

[9] Meaning magnetic field vectors with the same direction and sense

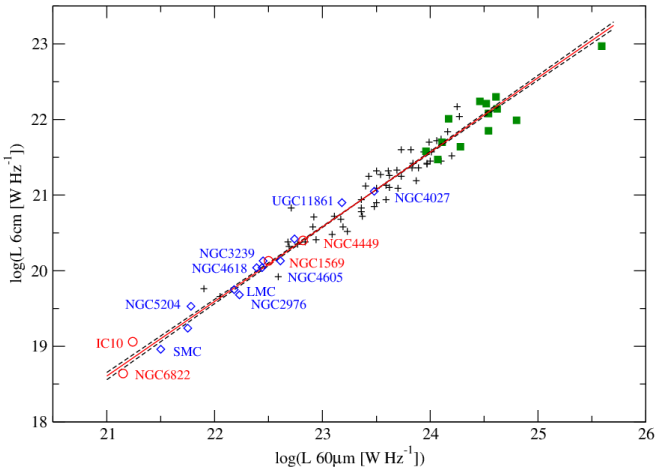

FIG. 11.— Radio–far-infrared correlation diagram for dwarf galaxies (circles), Magellanic-type and peculiar galaxies (diamonds), interacting objects (squares), and bright spiral galaxies (crosses). The luminosities at 4.85 GHz (6.2 cm) and at 60 μm are used, respectively. The solid line is a bisector fit to all (83) galaxies, while the dashed lines represent simple X vs. Y and Y vs. X regressions. Uncertainties in measurements are of the order of the symbols' sizes. The index of the power-law from the bisector fit is 0.99 ± 0.02.

the observer. With a density of thermal electrons of 0.1 cm^{-3} and the synchrotron path length of 1 kpc, such an RM value would indicate regular fields in this region of $\approx$ 2 ± 1 μG. Taking the path length two times smaller results in two times larger regular field strength.

With the present data we do not see any evidence for a galaxy-scale regular magnetic field in IC 10. We only found hints of local and relatively weak regular fields of about 2 μG strength in the giant H II complex. The existence of coherent structures of RM over large regions in IC 10 can further be investigated by independent sensitive spectropolarimetric observations, preferably at low radio frequencies to probe the extensive radio envelope. Application of RM synthesis is necessary to enable the separation of polarized signal coming from the Milky Way and IC 10. Such observations are feasible with LOFAR.

3.5. *Relation of Radio Emission of IC 10 to Other Galaxies*

We compare the radio emission of IC 10 with other galaxies using the radio–far-infrared (RFIR) diagram based on luminosities at 4.85 GHz and 60 μm, respectively. For the infrared emission of IC 10 we adopt a value of 33.5 Jy from Fullmer & Lonsdale (1989). To construct the RFIR relation, we use dwarf galaxies (NGC 6822, NGC 4449, NGC 1569), low-mass objects that we recently observed (NGC 2976, NGC 3239, NGC 4027, NGC 4605, NGC 4618, NGC 5204, UGC 11861), and five other Magellanic-type galaxies (Jurusik et al. 2014), 54 bright spirals from Gioia at al. (1982), and 13 objects from our compilation of interacting galaxies (Drzazga et al. 2011).

Our investigation shows (Fig. 11) that IC 10 does not deviate from the power-law fit constructed for all 83 galaxies of various types. It resides at the low-luminosity end of the relation, where galaxies of low mass and small total SFR are located. In this respect it is similar to the SMC. However, IC 10 has a high value of the surface density of star formation and strong magnetic fields (Sect. 4.1), similar to the starbursting dwarfs NGC 4449 and NGC 1569, which are larger, more massive, and more luminous than IC 10 (see Chyży et al. 2011). The total radio and infrared power of IC 10 is therefore not spectacular, but the local properties of the ISM are probably much like those in more massive starbursting dwarfs. They all could be triggered by gravitational interactions with other objects (see Sect. 1).

TABLE 3
MAGNETIC FIELD STRENGTH AND DEGREE OF FIELD ORDER IN IC 10

Region	B_{tot} μG	B_{ord} μG	Degree of Field Order
Whole galaxy	13.5 ±4.1	2.3 ± 0.7	0.17 ± 0.07
Giant H II complex	28.7 ± 8.6 (38.0[a])	1.6 ± 0.5	0.06 ± 0.03
North H II complex	28.4 ± 8.5 (39.9[a])	1.6 ± 0.5	0.06 ± 0.03
Tangle region	15.4 ± 4.6	1.3 ± 0.3	0.08 ± 0.05
H I hole 2	9.0 ± 2.7	1.0 ± 0.3	0.11 ± 0.05
H I hole 5	7.1 ± 2.1	3.5 ± 1.1	0.56 ± 0.24
H I hole 7	10.4 ± 3.1	2.7 ± 0.8	0.27 ± 0.12
Nonth. superbubble	22.0 ± 6.6	3.2 ± 1.0	0.15 ± 0.06
South PI extension	13.0 ± 3.9	4.7 ± 1.4	0.39 ± 0.17
Northern outskirts	8.6 ± 2.6	2.6 ± 0.8	0.32 ± 0.14
Southern outskirts	10.5 ± 3.2	2.3 ± 0.7	0.22 ± 0.09
Halo edge (1.4 GHz)	7.0 ± 2.1	n.a.	n.a.

[a] - Local value of the magnetic field strength after subtracting the influence of the background (disk) emission

4. DISCUSSION

4.1. *Magnetic Field Strength*

Our observations revealed that IC 10 possesses a diffuse, weak radio envelope and an unusual magnetic field morphology. In order to investigate the properties of the magnetic field further, we calculate global and local values of its strength and compare them with other galaxies. To this end, we use the combined VLA and Effelsberg 4.86 GHz data at 18″ angular (equivalent to 70 pc) resolution. For the calculation of the average magnetic field strength we assumed a thermal fraction of 0.5 and a nonthermal spectral index of $\alpha_{nth} = -0.6$, following Chyży et al. (2003). To derive local values, we make use of the nonthermal map (Fig. 9), assuming $\alpha_{nth} = -0.6$ within H II regions and $\alpha_{nth} = -0.8$ outside of them (see Heesen et al. 2015). A disk thickness of 1 kpc was used as the integration length along the line of sight. The calculations were performed with the standard assumption of energy equipartition between the magnetic field and total CRs, assuming a proton-to-electron ratio of 100 (Beck & Krause 2005).

We find an average total magnetic field strength of B_{tot} = 14 μG, which is stronger than in other low-mass galaxies (see, e.g., Chyży et al. 2011; Jurusik et al. 2014). With the help of the polarized emission, we also estimate the strength of the ordered field as B_{ord} = 2.3 ± 0.7 μG and that of the random field component as B_{ran} = 13.3 ± 4.0 μG. The degree of field order is $q = B_{ord}/B_{ran}$ = 0.17 ± 0.07, which is lower than typically observed in spiral galaxies. Our value is, however, in close agreement with the mean degree of field order of 0.27 ± 0.09, estimated for a sample of interacting galaxies showing kinetically disordered disks (Drzazga et al. 2011).

The strongest magnetic field is observed locally in the bright part of the southern giant H II complex with B_{tot} = 29 μG (Table 3). A similar value is found in the northern H II complex, which is also bright in Hα, but less extended. Generally speaking, regions with weak Hα emission have also weak field strengths, as, for instance, does the "tangle region," where B_{tot} = 15 μG (see Fig. 5 for a nomenclature of the regions). Inside holes of the H I distribution, which are in the vicinity of the brightest star-forming regions

(Wilcots & Miller 1998, see also Fig. 5), the magnetic field strength is halved in comparison with the surrounding area. In the nonthermal superbubble, the magnetic field is still strong (B_{tot} = 22 μG) and dominated by the random component (the degree of field order q = 0.15).[10] The superbubble is filled with CR electrons stemming from between one and a few supernova explosions, which occurred approximately 1 Myr ago (see Heesen et al. 2015). Because the nonthermal spectral index inside the bubble is significantly steeper, compared with surrounding areas, it is likely that the CR electrons are contained within and not able to freely escape. In the adjacent area to the south of this H II region, the magnetic field strength gradually decreases to B_{tot} = 13 μG while becoming more ordered (q = 0.39). If this region is also supplied with some CRs from the giant H II complex, the rising field order may suggest stretching of magnetic fields and diffusion of CRs along them to the south. Because in the northern and southern outskirts of IC 10 the magnetic fields have similar properties (see Table 3), the global outflow of magnetized plasma and stretching of the magnetic field in the whole observed radio envelope can explain the observed field strengths.

We also determined the strength of the total magnetic field in areas farthest away from the disk in the halo, which fall below the detection threshold at 4.86 GHz. We used the 1.43 GHz map and assumed that the thermal emission is negligible at the edge of the galaxy halo. For the synchrotron path length we adopted a value of 0.5 kpc, expecting a smaller path at the halo edge. Under these conditions, our estimations give total magnetic field strengths in the range of 6.8–7.1 μG, both in both the northern and southern halo, approximately 1.4 kpc away from the giant H II complex. Adopting the less likely value of 1 kpc for the path length results in diminishing the field strength by only 16%. In spite of the large distance from the galaxy disk, far away from the warm and hot ionized medium phases of the ISM, there is magnetized plasma with still strong magnetic fields.

While estimating the magnetic field strength as described above, it was assumed that in IC 10 synchrotron cooling dominates CR electrons' energy losses. But, in the galaxy's outskirts the inverse Compton scattering may become important and cool relativistic electrons, because the magnetic field energy density may become comparable to the photon energy density of the cosmic microwave background. This is the case when the total magnetic field strength drops below 3.25 μG$(1+z)^2$. But according to our estimations in low-level radio emission regions of IC 10 (to the north and to the south of the disk), using the above assumptions, the magnetic field strength is 7–10 μG (Table 3). This suggests that in the outer parts of the galaxy losses by inverse Compton scattering are always smaller than synchrotron losses, which justifies the way we estimate the radiative cooling of CR electrons. In the disk, inverse Compton losses are probably higher owing to photons from the galaxy's radiation field, so that our estimate of the electron radiation losses in the disk should be treated as a lower limit.

4.2. *Magnetic Field Structure*

As was shown in section 3, the magnetic topology in the outer disk of IC 10 resembles the X-shape — a magnetic field

[10] We refer to the superbubble as the entire structure along the line of sight (assumed here to be here 1 kpc) in the direction of the superbubble. Heesen et al. 2015 assumed that the superbubble only extends 153 pc along the line of sight and thus arrived at a higher magnetic field strength of 44 ± 8 μG.

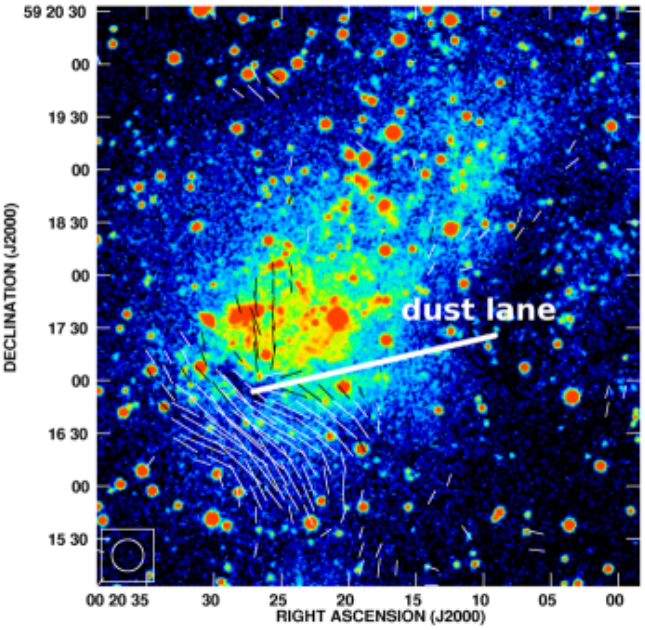

FIG. 12.— Magnetic field vectors of polarized intensity (from the combined VLA and Effelsberg data of 18″ resolution) of IC 10 superimposed on the DSS blue image. A vector of 10″ length corresponds to the polarized intensity of about 38 μJy beam^{-1}. The position of the strong dust lane is indicated.

structure dominated by the radial component, observed commonly in edge-on spiral galaxies (see, e.g. Tüllmann et al. 2000; Soida et al. 2011). As the observed vectors at 8.46 GHz (where the Faraday effects are small) have orientations in the radio halo similar to those at 4.86 GHz, they likely represent the true orientations of the magnetic field in projection onto the sky plane. In the northeastern part of the object, the B-vectors apparently form an elongated and curved structure. A similar field curvature can be seen in the opposite direction, around the polarized extension (Fig. 6). There is also a weak trace of B-vectors roughly aligned with the galaxy optical disk (PA = 125°).

Numerical MHD simulations show that in spirals the observed X-structures of magnetic fields could arise from the quadrupolar mode of the large-scale (α–Ω) dynamo (Beck et al. 1996), with the galactic wind transporting magnetic flux from the disk into the halo (Brandenburg et al. 1993; Moss et al. 2010). The poloidal component of the quadrupolar field alone cannot explain the X-shaped field, as according to the mean-field dynamo theory it is about 10 times weaker than the azimuthal disk field. Therefore, the vertical outflow is needed. Simulations of the CR-driven dynamo that include strong vertical winds (blowing with the speed exceeding 100 km s^{-1}) reveal the X-shaped structure in the edge-on view of spirals (Hanasz et al. 2009).

For the first time we find a similar X-pattern of magnetic fields in the dwarf galaxy IC 10, which is a stellar system with a highly irregular distribution of star-forming regions, does not reveal spiral density waves, and has a highly disturbed H I velocity field. Is the operation of a large-scale dynamo still possible in IC 10 to produce such fields? The efficiency of generation of the magnetic field can be roughly estimated from the dynamo number, according to the following equation:

$$D \approx 9\frac{h_0^2}{u_0^2} s\omega \frac{\partial \omega}{\partial s} \quad (1)$$

where h_0 is the vertical scale height of the galactic disk, u_0 is the velocity of turbulent motions, ω is the angular velocity at the radial distance s from the center of the galaxy, and $s\partial\omega/\partial s$ is the shear. In our calculations we assume $s = 0.5$ kpc and a velocity of rotation of about 30 km s^{-1} at a distance of 0.8 kpc, where the rotation curve is flat (Wilcots & Miller 1998). This gives a shear of 38 km s^{-1} kpc^{-1}. The velocity of turbulent motions we approximate by the velocity dispersion, which is about 30–40 km s^{-1} in the central part of the disk (Wilcots & Miller (1998). These values yield a dynamo number $|D| \approx 4$ which is below the critical value of ≈ 10. Therefore, the classical α–Ω dynamo cannot work in IC 10.

The numerical MHD simulations by Siejkowski et al. (2012) show that in a dwarf galaxy rotating with a velocity of about 30 km s^{-1} the CR-driven dynamo produces a regular magnetic field of only about 1 μG strength. Owing to the slow rotation of the gas, the e-folding time for developing such a field is quite long, about 800–1700 Myr, and can hardly explain magnetic fields in IC 10 as this is longer than the duration of the current starburst (10 Myr). The magnetic structure seen in IC 10 also does not resemble any numerical models simulated for dwarf galaxies (Dubois & Teyssier 2010; Siejkowski et al. 2012; Siejkowski et al. 2014). None of the models predict magnetic fields of the strength and vertical alignment as we observe in IC 10. It might be that gravitational interactions and gas accretion play an important role in the generation and evolution of the field in IC 10, which was not the emphasis of numerical simulations of dwarf galaxies so far.

Therefore, we propose another possibility to explain the magnetic X-pattern in IC 10: spreading and ordering of anisotropic magnetic fields by a global gas outflow, e.g. by a galactic wind (see Sect. 4.3). In this scenario, a large random component of the magnetic field is produced by a small-scale fluctuating dynamo and locally ordered by gas flows. The small-scale MHD dynamo can be sustained by the intensive phase of star formation visible in Hα emission. A comparison of the B-vectors with the distribution of H II-emitting gas gives the impression that the whole magnetic structure could be dominated by outflows just from the southern giant H II complex. This region is the youngest and most vivid star-forming area in the galaxy, as, e.g., it shows the bulk of W-R stars and harbors the bulk of the hot, X-ray-emitting gas (Wang et al. 2005). If this is the case, we might see in IC 10 large fragments of magnetic loops anchored to this region, similarly to the ones found in the 30 Doradus giant star formation region in the Large Magellanic Cloud (Mao et al. 2012). This would easily explain some curvatures of field lines visible on different sides of the galaxy. However, this appealing idea cannot easily explain the highly symmetric distribution of the radio intensity observed at 1.43 GHz, which indicates that the CRs and the magnetic field originate from the entire disk, rather than from only the southern part. One can speculate that the X-pattern is not directly related to the radio halo seen at 1.43 GHz, being a more recent phenomenon, associated mainly with the most prominent region of the current star formation burst. The radio halo could originate from the outflow triggered by the previous star-forming activity dated to have occurred at least 150 Myr ago (see Sect. 1).

The only polarized structure that appears to be unrelated to the global X-shaped pattern is the polarized region in the southern part of the object. For a more precise analysis we corrected the magnetic field orientation at 4.86 GHz for Faraday rotation using a map of the RM between 4.86 and 8.46 GHz. Owing to restricted polarized signal at 8.46 GHz, this was possible only in the southern part of the galaxy (Fig. 12). The orientations of the vectors closely resemble the low-resolution but high-frequency (10.55 GHz) magnetic structure obtained from the Effelsberg data (Chyży et al. 2003). The magnetic vectors seem to be unrelated to either the Hα or H I emission but are closely aligned with a long dust lane visible to the south from the giant H II complex (Fig. 12). Such a configuration of magnetic field lines could suppress the diffusion of CR electrons into areas southeast of the nonthermal superbubble (perpendicular to the field lines), which would explain the strong gradient of radio emission seen in this region at 1.43 GHz (Fig. 3).

TABLE 4
Radio Emission Scale Length and Wind Velocities in IC 10

Direction	Scale Length (kpc)	B_{tot} (μG)	t_{syn} (Myr)	V_w (km s^{-1})
1.43 GHz				
All	0.26	13.5	17.9	26 ± 4
NE (PA = 35°)	0.25	13.5	17.9	25 ± 4
NE from northern H II complex	0.29	20.0	9.9	52 ± 8
4.86 GHz				
All	0.19	13.5	9.7	35 ± 5
NE (PA = 35°)	0.17	13.5	9.7	30 ± 5
NE from northern H II complex	0.20	20.0	5.4	66 ± 10

It is also possible that some additional compression or stretching forces are at work here as well. According to recent investigations by Nidever et al. (2013), IC 10 is likely gravitationally interacting with another dwarf galaxy, which could induce various gas flows modifying the magnetic field morphology. Magnetic field lines aligned with the most pronounced dust lane in the galaxy might be of a very recent origin, probably from the ongoing starburst, which started only 10 Myr ago. Another process that could lead to field ordering is ongoing accretion of primordial gas, proposed to explain the complicated H I morphology of the object (Wilcots & Miller 1998).

Summarizing, there are probably several processes that shape the magnetic field structure in IC 10: first, compression and stretching in the vicinity of the expanding nonthermal superbubble in conjunction with gas flows, either from accretion of primordial gas or induced by recent tidal interaction: second, gas outflows from compact star-forming H II regions with a range of intensities, leading to a very localized (tens of parsec) velocity field; third, a galactic wind (1 kpc scale), driven by stellar winds from young, massive stars and supernova explosions. Spectropolarimetric observations in a wide range of frequencies are definitely needed to obtain more complete information on Faraday rotation and thus on intrinsic orientations of the magnetic field and to draw more robust conclusions about any external influences, possibly also responsible for the magnetic field structure in IC 10.

4.3. *Magnetized Galactic Winds*

The morphology of both the total power and PI, presented in Section 3, suggests that the magnetic field in IC 10 is probably, at least partially, shaped by a global galactic wind. The galactic halo that is well visible at 1.43 GHz map is not seen in any other ISM component. However, the expected hot gas in the halo (of 10^6 K) may exist but is not detected in soft X-rays owing to possible large absorption in the Milky Way

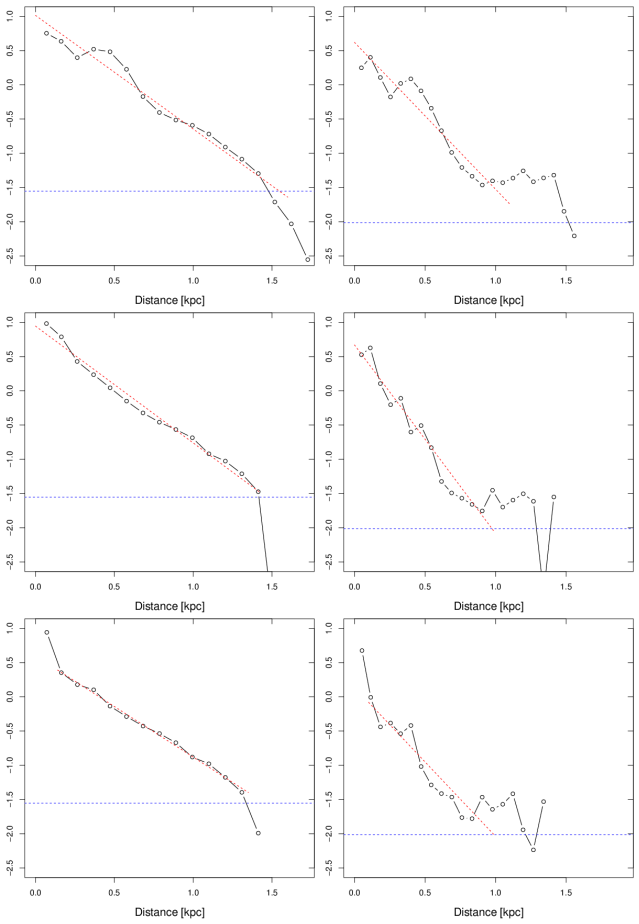

FIG. 13.— Radio emission profiles of IC 10 at 1.43 GHz (left) and 4.86 GHz (right) with fitted exponential models (see text for details). The top panels correspond to all directions from the galactic center; the middle panels to directions within the 45°sector around $PA = 35°$; the bottom panels to directions as in the middle ones, but with the tip of sectors moved to the northern giant H II complex. The horizontal lines mark the rms noise levels of the radio maps.

(see Sect. 3.3). Therefore, the radio emission and magnetic field structure remain the main evidence for a galactic wind in IC 10.

The detection of magnetic fields far from star-forming regions indicates that also a population of CRs is delivered to distant regions in the halo of IC 10. CRs can even drive thermal gas outflows with coupling facilitated by streaming instability (e.g. Dorfi & Breitschwerdt 2012).

Using the radio data, we will now attempt to estimate the bulk speed of the CR electrons, which are assumed to be transported convectively from the disk into the halo. We use the approach pioneered by Heesen et al. (2009), in which the bulk speed V_w of the wind can be approximated as the ratio of CR electrons' scale length l_e to the CR electron lifetime. The value of l_e can be derived from the synchrotron scale length (l_{syn}) in case of energy equipartition according to

$$l_e = \frac{3 - \alpha_{nth}}{2} l_{syn} \quad (2)$$

where α_{nth} is the nonthermal spectral index. For IC 10 we have $\alpha_{nth} \approx -0.6$ (Chyży et al. 2003).

The scale length l_{syn} is determined by fitting an exponential model to radial profiles, for which we integrated the radio emission in the sky plane in radial rings. Because in IC 10 the distributions of Hα and H I are very irregular and galactic disk orientation unclear (Sect. 4.2), we performed the fitting in three cases. First, we integrated emission over all azimuthal angles in rings centered on the optical center of the galaxy. Second, we included emission only from a sector with an opening angle of 45° and a major-axis orientation at $PA = 35°$. This sector is free of star-forming regions far from the disk, contrary to, e.g., the opposite (southeastern) direction, which shows the chain of H II regions (Sect. 3). In the third approach we made a similar fit but with the tip of the sector shifted to the center of the northern giant H II complex. This case seems to be the most reasonable one to measure the advection of plasma as the H II complex is probably the place of sources of CR acceleration and the magnetic field amplification process. The profiles of radio emission at 1.43 and 4.86 GHz and results of model fitting are given in Fig. 13 and Table 4. The obtained scale lengths for IC 10 of about 0.3 kpc at 1.43 GHz are significantly smaller than for massive spirals, e.g. NGC 253, for which the scale is about 1.7 kpc at the same frequency (Heesen et al. 2009).

For the estimation of the bulk speed of CR electrons we assume predominance of the synchrotron losses ($t_e = t_{syn}$). As stated earlier, inverse Compton scattering is neglected in our analysis, so that the actual electron lifetimes may be shorter. We also neglect adiabatic losses, which could further shorten the electron lifetimes and enlarge the derived velocity of the convective transport. The value of t_{syn} can be calculated from the formula

$$\frac{t_{syn}}{\mathrm{yr}} = 8.352 \times 10^9 \left(\frac{E}{\mathrm{GeV}}\right)^{-1} \left(\frac{B}{\mu\mathrm{G}}\right)^{-2} \quad (3)$$

where B is the strength of the total magnetic field (see Sec. 4.1) and E is the energy of the relativistic electrons derived at the frequency of observations ν:

$$\frac{E}{\mathrm{GeV}} = \left(\frac{\nu}{16.1\,\mathrm{MHz}}\right)^{0.5} \left(\frac{B}{\mu\mathrm{G}}\right)^{-0.5}. \quad (4)$$

Taking the scale lengths determined for various cases and using the above formula, we computed the bulk speed of CR electrons V_w (Table 4). The obtained values range from 25 to 66 km s^{-1}.

We approximate the escape velocity v_{esc} from the disk of IC 10 by the maximum velocity of galactic rotation: $v_{esc} \cong \sqrt{2}\, v_{max}$. Taking v_{max} of 30 km s^{-1} (Wilcots & Miller 1998), one gets v_{esc} of 40 km s^{-1}. Therefore, the estimated CR bulk speed in the vivid star-forming H II complex of 59 ± 13 km s^{-1} (a mean between 1.43 and 4.86 GHz values) is considerably higher than the escape velocity. The average values of V_w calculated for the whole galaxy or for northeast direction are slightly smaller (25–35 km s^{-1}) than the escape velocity. These two cases assume weaker magnetic fields, which leads to less energetic outflows of plasma from the galaxy disk. However, even in these cases it is conceivable that the CR bulk speed exceeds the escape velocity, because of our conservative estimate of the CR energy losses. This corroborates our earlier suggestion that a magnetized galactic-scale wind exists in IC 10.

A similar conclusion can be drawn from a rough estimate of the wind speed from the radial slope of the spectral index profile (see Heesen et al. 2009). In the northeastern direction from the northern H II complex the gradient of the spectral index between 1.43 and 4.86 GHz is about $\Delta\alpha/\Delta r = -1.1 \pm 0.1$ kpc^{-1}. For a magnetic field strength of $20 \pm 3\,\mu$G we first

derive the time derivative of the radio spectral index $\Delta\alpha/\Delta t$ and then obtain the bulk speed $V = \Delta r/\Delta t = 62 \pm 17\,\mathrm{km\,s^{-1}}$. This value agrees with the wind velocity obtained from the radio profiles.

In our approach we assumed that plasma is transported convectively from the disk into the halo. We can now justify this assumption observing that the vertical profiles of the 1.43 GHz radio continuum emission shown in Fig. 13 can be closely approximated by exponential functions, as expected for convection, whereas diffusion would lead to profiles resembling a Gaussian function (Heesen et al. 2009, 2016). This means that diffusion plays only a minor role, providing us with an upper limit of the diffusion coefficient as $D < (1-3)\times10^{27}\,\mathrm{cm^2\,s^{-1}}$ (assuming $D = l_e^2/t_e$ and conditions given in Table 4 for 1.43 GHz). This value is approximately a factor of 10 smaller than the Milky Way value (Strong et al. 2007), probably caused by the very turbulent magnetic field structure (Sect. 4.1).

Our estimate of the galactic outflow speed in IC 10 is in agreement with the outflow speeds in dwarf galaxies measured from the Na I D absorption line (below $100\,\mathrm{km\,s^{-1}}$), at least for those objects that have similar circular velocities and SFRs (Veilleux et al. 2005). Thus, the observed extensive magnetic fields in the halo of IC 10 are probably not produced "in situ" by a dynamo process, but are likely ejected from H II complexes and dragged along with the galactic wind.

Galactic outflows are also considered as one of the mechanisms to form large-scale X-shaped magnetic fields observed in edge-on spiral galaxies (Sect. 4.2). With a velocity of about $60\,\mathrm{km\,s^{-1}}$ the CRs and magnetic fields in IC 10, if advected with winds, can reach the most distant observable regions in the radio halo within 2×10^7 yr. This corresponds well to the timescale of the currently ongoing starburst (Sect. 1). The vertical extent of the radial (X-type) structure in IC 10, when compared with the optical disk size, is, relatively speaking, even larger than in edge-on spiral galaxies, such as NGC 4631 or NGC 5775. In typical late-type spiral galaxies, the radio halo extends vertically only above star-forming regions, i.e. galaxies have "sharp edges" (Dahlem et al. 2006). In IC 10, however, the magnetic structure fills the entire, almost spherical radio halo (Fig. 6). Hydrodynamic simulations of CR-driven winds by Uhlig et al. (2012) indeed predict that dwarf galaxies can experience spherically symmetric outflows. To fully compare such models with IC 10, the explicit treatment of magnetic fields is necessary.

There is yet another impact of the proposed large-scale magnetized wind in IC 10: galactic winds are considered as a potential process that enable galaxies to magnetize the IGM. Dwarf galaxies, which have shallow gravitational potentials and burst-like star formation histories, could spread magnetic fields into areas very remote from the regions of magnetic field and CR generation (Kronberg et al. 1999; Dubois & Teyssier 2010; Chyży et al. 2011). The radial topology of the ordered magnetic field in the halo of IC 10, which currently undergoes a starburst (see Fig. 12), enables efficient transport of the magnetized plasma along the open field lines and nicely conforms with this picture.

We trace the magnetic field in the halo of IC 10 out to a distance of about 1.4 kpc from the galaxy's center at 1.43 GHz. If the magnetized halo freely expands to a stall radius of about 5 kpc (see analytic modeling of Chyży et al. 2011), we expect still strong fields there of $\approx0.5\,\mu$G. Such extensive fields could be detected by probing very low energy CRs with low-frequency observations (with WSRT, GMRT, or LOFAR), or by the method of RM grids toward background polarized sources. Such observations would allow us to justify the role of starburst dwarf galaxies, such as IC 10, in the magnetization of the IGM. Local starbursting dwarf galaxies constitute the ideal laboratory for such studies, since they are, in the paradigm of the ΛCDM hierarchical structure formation, the closest analogs of the first galaxies in the Universe.

5. CONCLUSIONS

We present a multifrequency radio continuum polarimetry study (1.43, 4.86, and 8.46 GHz) of IC 10, the nearest dwarf irregular galaxy in an ongoing starburst phase. We use a combination of interferometric observations with the VLA and single-dish observations with the 100-m Effelsberg telescope. Our main conclusions are as follows:

1. Sensitive VLA observations at 1.43 GHz reveal a large radio envelope of IC 10 in total intensity, extending up to 1.4 kpc away from the galaxy's center, thus almost two times further than the infrared-emitting galactic disk. The envelope is not seen at higher frequencies (4.86 and 8.46 GHz), suggesting substantial aging of CR electrons, actually confirmed by a gradual steepening of the nonthermal spectral index with distance from the galactic disk.

2. Compared to the total radio emission, the polarized emission of IC 10 at 4.86 and 8.46 GHz is more clumpy, with the most pronounced polarized extension located in the southern part of the galaxy, partially corresponding to the nonthermal superbubble. At 1.43 GHz, the polarized signal covers also a large fraction of the observed area around the galaxy, which we explain as the Milky Way's foreground signal, unrelated to IC 10. Such a strong foreground polarized emission has not been found in any other external galaxy before.

3. On the largest scales, the apparent B-vectors of the PI exhibit a global "X-shaped" morphology of magnetic fields, with a dominating radial component. The structure resembles the one observed in several nearby edge-on spiral galaxies with higher SFRs. No such structures have been observed in dwarf galaxies to date. The X-shaped magnetic structure can be caused by galactic winds pulling out magnetic fields, driven by stellar winds from young, massive stars and supernova explosions.

4. At the northern edge of the nonthermal superbubble, the magnetic field orientation changes abruptly and is aligned with a prominent dust lane that can be seen in optical images. This reveals some external processes shaping the magnetic field, as infalling gas and/or tidal interactions, resulting in compressed or stretched magnetic field lines.

5. In spite of the small size and mass of IC 10, the magnetic field strength has a mean of $14\,\mu$G, similar to those found in massive spiral galaxies. What sets the magnetic field structure apart is the dominating random component with a degree of field order of only 0.17 ± 0.07, so that the ordered component has a mean strength of merely $2.3 \pm 0.7\,\mu$G. Locally, the field is strongest in the southern and northern bright H II complexes, where it reaches $29\,\mu$G and is almost entirely

random. Farther away from the star-forming sites, the magnetic field becomes gradually more ordered, while at the same time the field strength drops. The non-thermal superbubble and the "tangle region" have field strengths of 22 and 15 μG, respectively. In the centers of H I holes, the field strength is about 7–10 μG and of various degrees of field order (0.1–0.5). Even in the most distant galaxy outskirts (about 1.4 kpc from the center), the magnetic field is still strong (with strength of $\approx$7 μG) and partly ordered (with a degree of 0.2–0.3).

6. We detect Faraday rotation of about -150 ± 69 rad m^{-2} in the giant H II complex, which corresponds to a weak regular magnetic field of 2 ± 1 μG. We rule out a scenario for global operation of the mean-field dynamo process in IC 10, as the calculated large-scale dynamo number is subcritical and the e-folding time for amplification of the regular field is relatively long ($>8\times10^8$ yr, according to MHD simulations). Therefore, the strong total magnetic fields in IC 10 probably arise from the small-scale dynamo.

7. The radio emission profiles at 1.43 GHz indicate a scale length of the radio halo in IC 10 of about 0.3 kpc, several times smaller than found in massive spiral galaxies at the same frequency. In combination with the CR electron lifetime, this implies a CR bulk speed from regions dominated by a giant H II complex of about 60 km s^{-1}, exceeding the escape velocity. Thus, galaxy-wide magnetized winds can induce X-shaped magnetic fields and blow up the extensive radio halo visible in total intensity at 1.43 GHz. Moreover, the magnetized plasma escaping from the gravitational well of this dwarf irregular galaxy is able to seed random and ordered magnetic fields in the IGM, in a similar fashion that posited for the first low-mass galaxies in the early Universe.

The radio picture of IC 10 is complex and manifests some magnetic patterns, which were found previously only in massive spiral galaxies. Therefore, this dwarf irregular galaxy, one of our cosmic next-door neighbors that form the Local Group, is a valuable laboratory for our understanding of the generation and evolution of magnetic fields in galaxies in general. Because of IC 10's close proximity, it can serve as one of the benchmarks at which realistic numerical MHD simulations of the ISM and galactic outflows can be tested against. IC 10 holds valuable clues as to how low-mass galaxies acquire gas for triggering starbursts and how they amplify magnetic fields and eventually spread them out into the IGM. Having a clumpy disk and an intense star-forming activity, which provides significant feedback to the magnetized plasma, it allows us to gain precious insight in processes that regulate the formation of protogalaxies in the early Universe.

We are thankful to Aritra Basu and the anonymous referee for very useful comments. This work was supported by the Polish National Science Center grant No. 2011/03/B/ST9/01859 (observations) and 2012/07/B/ST9/04404 (simulations and analysis). V.H. acknowledges support from the Science and Technology Facilities Council (STFC) under grant ST/J001600/1. R.B. and D.J.B. acknowledge support by the DFG Research Unit FOR1254. We acknowledge the use of the HyperLeda (http://leda.univ-lyon1.fr) and NED (http://nedwww.ipac.caltech.edu) databases.

REFERENCES

Ashley, T., Elmegreen, B. G., Johnson, M., et al. 2014, AJ, 148, 130
Beck, R., Brandenburg, A., Moss, D., Shukurov, A., & Sokoloff, D. 1996, ARA&A, 34, 155
Beck, R., & Krause, M. 2005, AN, 326, 414
Beck, R., & Wielebinski, R. 2013, arXiv:1302.5663
Bendo, G. J., Gilliano, F., & Madden, S. C. 2012, MNRAS, 423,197
Brandenburg, A., Donner, K.J., Moss, D., Shukurov, A., Sokoloff, D.D., & Tuominen, I. 1993, A&A, 271, 36
Caplan, J., & Deharveng, L. 1986, A&A, 155, 297
Chyży, K.T., Knapik, J., Bomans, D. J., Klein, U., Beck, R., Soida, M., & Urbanik, M. 2003, A&A, 405, 513
Chyży, K.T., Bomans, D.J., Krause, M., Beck, R., Soida, M., & Urbanik, M. 2007, A&A, 462, 933
Chyży, K.T., Ehle, M., & Beck, R. 2007, A&A, 474, 415
Chyży, K. T., Weżgowiec, M., Beck, R., & Bomans, D. 2011, A&A, 529, A94
Dahlem, M., Lisenfeld, U., &Rossa, J. 2006, A&A, 457, 121
Dorfi, E. A., & Breitschwerdt, D. 2012, A&A 540, A77
Drzazga, R.T., Chyży, K.T., Jurusik, W., & Wiórkiewicz, K. 2011, A&A, 533, 22
Dubois, Y., & Teyssier, R. 2010, A&A, 523, A72
Dumke, M., Krause, M., Wielebinski, R., & Klein, U. 1995, A&A, 302, 691
Emerson, D. T., & Gräve, R. 1988, A&A, 190, 353
Emerson, D. T., Klein, U., & Haslam, C. G. T. 1979, A&A, 76, 92
Fullmer, L., & Lonsdale, C. J. 1989, JPL D-1932, Version 2, Part no 3
Gil de Paz, A., Madore, B.F., & Pevunova, O. 2003, ApJS, 147, 29
Gioia, I. M., Gregorini, L., & Klein, U. 1982, A&A, 116, 164
Grebel, E. K., Gallagher, J. S. III, & Harbeck, D. 2003, AJ, 125, 1926
Hanasz, M., Wóltański, D., & Kowalik, K. 2009, ApJ, 706, L155
Haslam, C. G. T. 1974, A&AS, 15, 333
Heald, G., Braun, R. & Edmonds, R. 2009, A&A, 503, 409
Heesen, V., Beck, R., Krause, M., & Dettmar, R.J. 2009, A&A, 494, 563
Heesen, V., Rau, U., Rupen, M.P., Brinks, E., & Hunter, D.A. 2011, ApJ, 739, L23
Heesen, V., Brinks, E., Krause, M. et al. 2015, MNRAS, 447, L1
Heesen, V., Dettmar, R.-J., Krause, M, Beck, R & Stein, Y. 2016, MNRAS, submitted
Hunter, D.A., Ficut-Vicas, D. Ashley, T., et al. 2012, ApJ, 144, 134
Jurusik, W., Drzazga, R. T., Jableka, M., Chyży, K. T., Beck, R., Klein, U., & Weżgowiec, M. 2014, A&A, 567, A134
Kronberg, P.P., Lesch, H., & Hopp, U. 1999, ApJ, 511, 56
Leroy, A., Bolatto, A., Walter, F., & Blitz, L. 2006, ApJ, 643, 825
Lozinskaya, T.A., & Moiseev, A.V. 2007, MNRAS, 381, 26
Mao, S. A., McClure-Griffiths, N. M., Gaensler, B. M., et al. 2012, ApJ, 759, 25
Massey, P., & Armandroff, T. E. 1995, AJ, 109, 2470
Massey, P., Olsen, K. A. G., Hodge, P. W., et al. 2007, AJ, 133, 2393
Mateo, M. 1998, ARA&A, 36, 435
Mora, S. C., & Krause, M. 2013, A&A, 560, A42
Moss, D., Sokoloff, D., Beck, R., & Krause, M. 2010, A&A, 512, A61
Mulcahy, D. D., Horneffer, A., Beck, R., et al. 2014, A&A, 568, A74
Nidever, D.L., Ashley, T., Slater, C.T., et al. 2013, ApJ, 779, 15
Oppermann, N., Junklewitz, H., Robbers, G., et al. 2012, A&A, 542, A93
Perley, R. A., & Butler, B. J. 2013, ApJS, 204, 19
Recchi, S., & Hensler, G. 2013, A&A, 551, A41
Sanna, N., Bono, G., Stetson, P.B. et al. 2008, ApJ, 688, L69
Sault R.J., Teuben P.J., & Wright M.C.H. 1995, in Astronomical Data Analysis Software and Systems IV, ed. R. A. Shaw, H.E. Payne, J.J.E. Hayes, ASP Conference Series, 77, 433
Siejkowski, H. 2012, PhD thesis, Jagiellonian University, Kraków
Siejkowski, H., Otmianowska-Mazur, K., Soida, M., Bomans, D. J., & Hanasz, M. 2014, A&A, 562, A136
Soida, M., Krause, M., Dettmar, R.J., & Urbanik, M. 2011, A&A, 531, 127
Strong, A. W., Moskalenko, I. V., & Ptuskin, V. S. 2007, Annual Review of Nuclear and Particle Science, 57, 285
Thurow, J. C., & Wilcots, E. M., 2005, ApJ, 129, 745
Tüllmann R., Dettmar, R.-J., Soida, M., Urbanik, M., & Rossa, J. 2000, A&A, 364, L36

Uhlig, M., Pfrommer, C., Sharma, M., Nath, N., N., Enslin, T. A., & Springel, V., 2012, MNRAS, 423, 2374
Vacca, W. D., Sheehy, C D., & Graham, J. R. 2007, ApJ, 662, 272
Veilleux, S., Cecil, G., & Bland-Hawthorn, J. 2005, ARA&A, 43, 769
Wang, Q. D., Whitaker, K. E., & Williams, R. 2005, MNRAS, 362, 1065
Wilcots, E.M., & Miller, B.W. 1998, AJ, 116, 2363
Yang, H., & Skillman, E.D. 1993, AJ, 106, 1448